PROCEEDINGS A

royalsocietypublishing.org/journal/rspa

Research

Cite this article: Armand J, Pesaresi L, Salles L, Wong C, Schwingshackl CW. 2019 A modelling approach for the nonlinear dynamics of assembled structures undergoing fretting wear. *Proc. R. Soc. A* **475**: 20180731. http://dx.doi.org/10.1098/rspa.2018.0731

Received: 23 October 2018
Accepted: 14 February 2019

Subject Areas:
computational mechanics, mechanical engineering

Keywords:
contact modelling, fretting wear, roughness

Author for correspondence:
Luca Pesaresi
e-mail: luca.pesaresi12@imperial.ac.uk

A modelling approach for the nonlinear dynamics of assembled structures undergoing fretting wear

J. Armand[1], L. Pesaresi[1], L. Salles[1], C. Wong[2] and C. W. Schwingshackl[1]

[1]Imperial College London, London, SW7 2AZ, UK
[2]Rolls-Royce plc, Derby, DE2 48J, UK

LP, 0000-0003-2059-4574

Assembled structures tend to exhibit nonlinear dynamic behaviour at high excitation levels due to the presence of contact interfaces. The possibility of building predictive models relies on the ability of the modelling strategy to capture the complex nonlinear phenomena occurring at the interface. One of these phenomena, normally neglected, is the fretting wear occurring at the frictional interface. In this paper, a computationally efficient modelling approach which enables considerations of the effect of fretting wear on the nonlinear dynamics is presented. A multi-scale strategy is proposed, in which two different time scales and space scales are used for the contact analysis and dynamic analysis. Thanks to the de-coupling of the contact and dynamic analysis, a more realistic representation of the contact interface, which includes surface roughness, is possible. The proposed approach is applied to a single bolted joint resonator with a simulated rough contact interface. A tendency towards an increase of real contact area and contact stiffness at the interface is clearly observed. The dynamic response of the system is shown to evolve over time, with a slight decrease of damping and an increase of resonance frequency, highlighting the impact of fretting wear on the system dynamics.

1. Introduction

In aerospace applications, high-performance structural analysis is needed to provide accurate predictions of the vibratory response levels of various components [1].

THE ROYAL SOCIETY PUBLISHING

In particular, assembled structures are characterized by contact interfaces which are a source of damping and can alter the dynamics of the system [2]. For this reason, a standard linear analysis is not enough, and nonlinear analysis is necessary to capture the more complex dynamic behaviour. One of the most common approaches to model this class of dynamic problems with contact relies on the use of harmonic balance method (HBM) solvers to calculate the steady-state nonlinear response of the system [3]. From initial studies with lumped mass models [4], and thanks to the development of powerful reduction techniques [5], it has then been possible to study more realistic structures using large-scale finite-element models. In order to include the contact nonlinearity in the model, the contact interface is commonly discretized with a grid of three-dimensional (3D) node-to-node Jenkins elements [6,7] or alternatively either one or a few micro-slip elements [8,9]. One main simplification of these models is that the interfaces are smooth, and the contact parameters are simply 'tuning' factors. More recent attempts [10,11] have tried to address this, by developing new approaches to include the effect of roughness in the dynamic simulations and link the contact parameters to the micro-mechanics of the contact. Despite the significant research efforts, the vast majority of the proposed modelling approaches rely on the main simplification that the contact interface does not change over time. This simplification clearly does not correspond to reality, as fretting wear due to the oscillatory dynamic loadings will cause a modification of the interface.

A large number of wear models has been developed in the past with the Archard's law being a recognized and well-accepted reference [12]. In the last decade, some researchers such as Fouvry *et al.* [13] have investigated the link between the wear response and the energy dissipation of a tribo-system. Starting from the idea that friction and wear are irreversible processes which disorder a system and generate entropy, several researchers have developed a variety of thermodynamic models [14,15]. Although these latter approaches can better capture the complexity of the wear phenomena, the large number of parameters and variables required for their calculations make their use impractical for many applications. In addition to a wear model, computational techniques are required to solve the contact problem and predict the amount of wear. Several different techniques have been used, including finite-element method (FEM) [16], boundary element method (BEM) [17], finite-discrete element method (FDEM) [18] and molecular dynamics (MD) [19].

Although the study and modelling of fretting wear is an established research field on its own, very few attempts have been made to include fretting wear in dynamic models. For this reason, there is still a lack of understanding concerning the impact that fretting wear may have on the dynamic response of a system with frictional contacts. Some researchers, such as Sextro [20] or Pettigrew [21] focused on the evaluation of wear resulting from the vibrations of the system, rather than the effects of wear on the dynamics. Other studies investigated the effect of mistuning of bladed discs caused by the wear of underplatform dampers [22,23]. Salles *et al.* [24] proposed a multi-scale approach for the numerical treatment of vibrating structures undergoing fretting-wear. The key idea was the introduction of two different time scales, a slow one for the contact evolution and a fast one for the dynamic calculation. In this numerical study, the coupling between the dynamics and tribology caused by fretting wear was highlighted for the first time. It was shown that even small modifications of the surface (few micrometres) had an impact on the dynamic response of the system.

In this paper, a multi-scale approach to model the effect of fretting wear on the nonlinear dynamics of structures with frictional contacts is presented. In addition to the use of two time scales similarly to [24], two different space scales are also introduced for the contact and dynamic analysis. For this reason, a BEM-based contact solver is used which allows reproducing the contact roughness in details without increasing the computational cost required for the dynamic computation. The general idea of this approach was initially presented in [25], but was limited to smooth contacts and to a specific damper model application. In this paper, the approach is generalized to treat rough contacts, as this represents a fundamental step for a more physical description of contact interfaces. In fact, real engineering surfaces are rough at the micro-scale, and fretting wear causes a modification of the roughness characteristics of the interface, leading

to a different normal and tangential contact behaviour. This, in turn, may lead to a different dynamic response of the system. Therefore, it is believed that for a predictive dynamic model, surface roughness should be included to better capture the effect of wear on the evolution of the contact conditions.

2. Modelling approach

In the following sections, the general structure of the modelling approach is presented in details. The proposed approach unifies techniques that have been used for a while in their respective fields of nonlinear dynamics and contact mechanics in a new comprehensive framework. The proposed approach is then applied to a single lap joint resonator (see §3), and a detailed analysis of the results is shown in §4.

(a) General structure of the multi-scale approach

Fretting wear is a complex multi-scale phenomenon, and therefore a multi-scale approach seemed natural to tackle this problem. In the proposed multi-scale approach, two different discretizations of the contact are used for the dynamic and contact/wear analysis. A macro-scale is used for the dynamic simulations which require capturing the local deformations at the interface, whereas a meso- or micro-scale is used for the contact analysis, which allows capturing the fine details of the roughness. The same multi-scale strategy is used in time, where a fast scale is introduced for the dynamic analysis, whereas a slower scale is used for the tribological phenomena.

The proposed multi-scale approach is based on three separate tools: (i) a dynamic solver based on the multi-harmonic balance method, (ii) a contact solver based on boundary integral equations, that allows the inclusion of roughness in the contact analysis, and (iii) an energy wear approach to compute the contact evolution due to fretting wear. The general structure of the proposed approach is summarized in figure 1. It is worth noting that two assumptions were made in this approach for simplification:

— The depth of wear is considered to be very small relative to the characteristic dimensions of the structures in contact, which is why the changes due to wear of the mass and stiffness matrices used in the dynamic analysis are neglected. This assumption seems to be acceptable for most engineering structures apart from special micro- or nano-scale applications.
— The dynamic and refined contact analyses are solved separately and in an uncoupled iterative way. Therefore, wear is assumed to remain constant during the dynamic analysis, and similarly, the nonlinear dynamic contact forces are assumed to remain constant during the wear computations. This assumption is stronger, but it is necessary as it allows to significantly simplify the treatment of the problem. More details on the impact of this assumption are given in §2d(i).

In what follows, the nonlinear dynamic analysis §2b, the contact solver §2c and wear computation §2d are briefly described, and then their use within the general multi-scale approach is explained in detail §2e.

(b) Nonlinear dynamic analysis

The nonlinear dynamic response of the system is obtained using a multi-harmonic balance (MHBM) solver, which is implemented in the in-house code FORSE (FOrced Response SuitE). A detailed explanation of the methods used in the code can be found in [26,27], and only a brief overview is presented here. The main advantage of a frequency-based MHBM approach is that it allows a much faster computation of the nonlinear steady-state response of the system compared to time-domain approaches. The drawback is that transient phenomena cannot be captured with

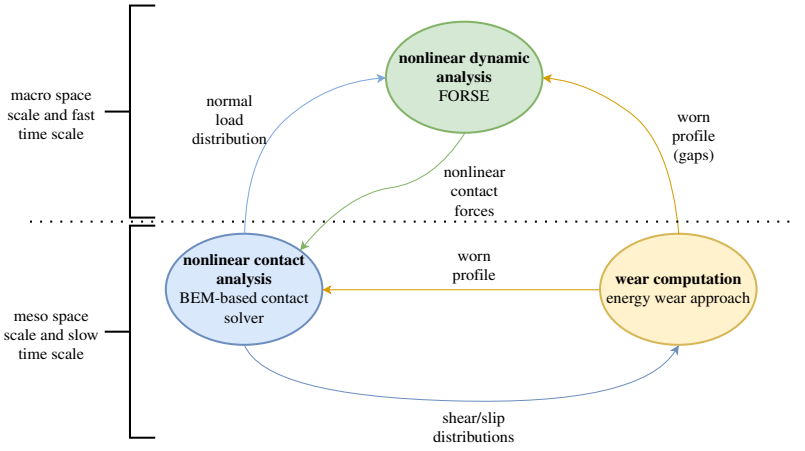

Figure 1. General scheme of the multi-scale modelling approach. (Online version in colour.)

the MHBM, and therefore the contact evolution due to wear cannot be 'embedded' directly in the model, but it needs to be treated separately (see §2e). When frictional interfaces are present in the system, the equations of motion become nonlinear, and can be written as follows:

$$\mathbf{M}\ddot{\mathbf{q}}(t) + \mathbf{C}\dot{\mathbf{q}}(t) + \mathbf{K}\mathbf{q}(t) + \mathbf{f}\left[\mathbf{q}(t), \dot{\mathbf{q}}(t)\right] = \mathbf{p}(t), \tag{2.1}$$

where $\mathbf{q}(t)$ is a vector of displacements for all degrees of freedom (d.f.s) in the system; $\mathbf{M}$ $\mathbf{C}$, $\mathbf{K}$, are the mass, damping and stiffness matrices of the linear model; $\mathbf{p}(t)$ is the harmonic external excitation to the system, and $\mathbf{f}[\mathbf{q}(t), \dot{\mathbf{q}}(t)]$ are the nonlinear friction forces at the interface. The main simplification of the MHBM is that the nonlinear displacements $\mathbf{q}(t)$ (and forces) are approximated by a restricted Fourier series, i.e.

$$\mathbf{q}(t) = \mathbf{Q}_0 + \sum_{j=1}^{n} \left(\mathbf{Q}_j^c \cos m_j \omega t + \mathbf{Q}_j^s \sin m_j \omega t \right), \tag{2.2}$$

where $\mathbf{Q}_j^{c,s}$ are the harmonic coefficients of the degrees of freedom of the system, n is the number of harmonics that are used in the multi-harmonic expansion, and ω is the fundamental pulsation of the excitation. In order to allow a faster computation, a hybrid reduction method [27] is used, which allows to significantly reduce the size of the problem. The flow chart with the different steps required for the nonlinear dynamics calculations is shown in figure 2*a*. Prior to the analysis, a detailed finite-element modal analysis is performed to obtain the modal properties which are used for the model reduction. Following a common approach in many MHBM solvers, the contact forces are calculated in the time-domain using the alternating frequency-time method (AFT) [24,28] as shown in figure 2*b*. This allows a direct calculation of the contact forces, as well as a higher flexibility in the code in case different contact laws are implemented.

To allow an accurate physical description of the nonlinearity, the contact interface is discretized by using a dense grid of node-to-node 3D contact elements (figure 3). A detailed description of the 3D contact element for which analytical expressions of the stiffness matrix were obtained can be found in [26]. Each friction element is made of two coupled Jenkins elements [2] to model a two-dimensional in-plane motion, which are coupled to a spring in the normal direction. Six parameters characterize its properties: the element area A, the friction coefficient μ, the normal static load N_0, the normal static gap g_0 and the tangential k_t and normal k_n contact stiffness (also known as 'penalty' coefficients). All the contact parameters for each contact elements of the interface are obtained using the contact solver described in §2c. Only the friction coefficient is obtained experimentally (or from database), since it is very difficult to have a predictive model for it, which is largely beyond the scope of the present work.

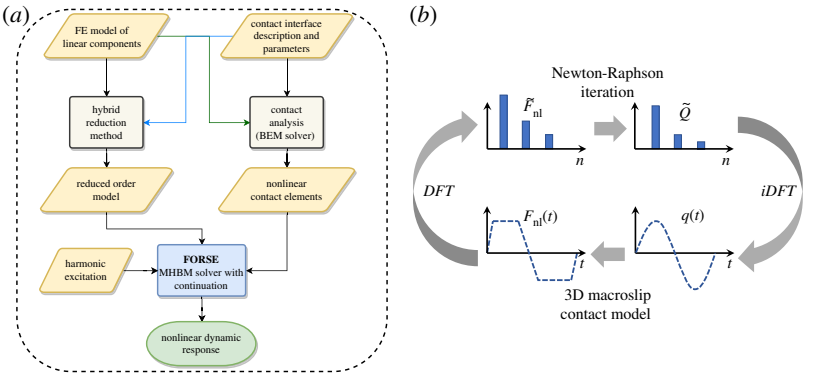

Figure 2. (*a*) Flow chart of the forced response analysis, (*b*) scheme of the alternate frequency-time (AFT) procedure. (Online version in colour.)

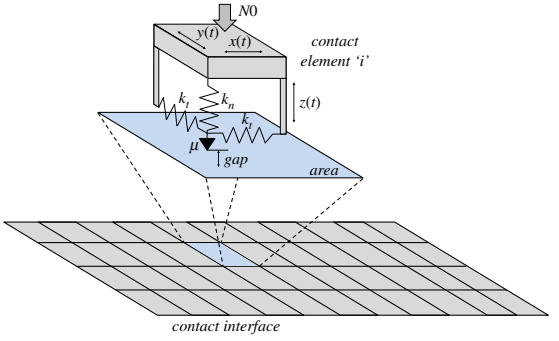

Figure 3. Contact discretization for the dynamic analysis. (Online version in colour.)

(c) Contact analysis

The contact analysis was performed independently of the dynamic analysis by means of a contact solver based on the BEM [25,29]. Thanks to the computational speed of the BEM-based contact solver a very refined contact mesh can be used compared to the mesh used for the dynamics, which allows to include roughness in the analysis. The contact solver implementation, which is described in details in [29], is based on the projected conjugate gradient method [30] and a discrete-convolution fast Fourier transform which speeds up the computation. The half-space assumption allows the use of the Boussinesq and Cerruti potentials [31,32] to compute the surface elastic deflections in the normal and tangential directions. The normal displacement u_z caused by a pressure distribution p are described by equation (2.3), whereas equation (2.4) is its discretized form on a regular grid of $N_x \times N_y$ points. Initially, the normal contact problem is solved using the conjugate gradient method, after which the tangential problem is solved with the Coulomb friction law as a bound to the shear distribution in the slipping region.

$$u_z(x,y) = \frac{1-\nu^2}{\pi E} \int_{-\infty}^{+\infty} \int_{-\infty}^{+\infty} \frac{p(\xi,\eta)}{\sqrt{(\xi-x)^2+(\eta-y)^2}} \,\mathrm{d}\xi \,\mathrm{d}\eta, \tag{2.3}$$

where E and ν are Young's modulus and Poisson ratio of the material, respectively.

$$u_z(i,j) = K_{zz} \otimes p = \sum_{k=1}^{N_x} \sum_{l=1}^{N_y} p(k,l) K_{zz}(i-k, j-l), \tag{2.4}$$

where $\otimes$ is the discrete convolution product and $K_{zz}(i,j)$ are the discrete influence coefficients [25] which are used to obtain the normal displacement resulting from unit pressure on the element (i,j).

(d) Wear computation

To evaluate the effect of fretting wear on the rough contact interface, the energy wear approach [13,33] is used. Although more refined wear models exist, as discussed in the introduction, the energy wear approach was selected as it allows a straightforward and fast calculation of the wear volume, and for this reason is particularly well suited in the framework of a multi-scale analysis. The main concept of this approach is that the total wear volume calculated after N_{cycles} is considered to be proportional to the dissipated energy:

$$V = \alpha \sum_{n=1}^{N_{\text{cycles}}} Ed_n, \tag{2.5}$$

where α is a wear coefficient and Ed_n is the frictional dissipated energy accumulated during the nth cycle. In order to perform a refined local contact analysis accounting for wear, a local form of equation (2.5) is used:

$$\Delta h_{ij} = \alpha \int_0^T \left\| \mathbf{q}_{ij}(t) \right\| \left\| \Delta \mathbf{v}_{ij}(t) \right\| \, \mathrm{d}t, \tag{2.6}$$

where Δh_{ij} is the wear depth at each node after one cycle, $\mathbf{q}_{ij}$ and $\Delta \mathbf{v}_{ij}$ are the tangential shear stresses and the relative tangential velocities at the point (i,j), T is the period of the vibration cycle and $\| \cdot \|$ is the Euclidean norm. The computed worn volume is removed from the contact area and the effects of the third body is not considered in this study. One of the drawbacks of this approach is that the accuracy of the wear computation is highly dependent on the estimation of the wear coefficient α. For this reason, the ability of the model to predict correct wear evolution strongly relies on the availability of dedicated fretting wear measurements, where the operating conditions of the systems studied have to be closely reproduced.

(e) Multi-scale analysis

The multi-scale approach, summarized in the flow chart in figure 4, is as follows. Initially, the BEM-based contact solver is used for the contact analysis in order to obtain the static pressure, gap distributions and normal and tangential contact stiffness of the rough contact interface. The input necessary for this first contact analysis is the total normal load, known to be transmitted through the contact area. These initial contact interface parameters are then associated with each contact element of the coarser mesh used for the dynamic analysis. More precisely, the pressure distribution of each 3D contact element is the sum of the normal load at each node of the contact analysis enclosed by the area of the 3D contact element, divided by that area. The contact stiffnesses are extracted from averaged normal load indentation and hysteresis curves, in which the normal and tangential loads are summed over all the nodes of the finer mesh, and the relative displacements are averaged. As for the gaps, the minimum gap value from the finer mesh was used in the 3D contact element. Subsequently, the MHBM solver is used for the dynamic response and to obtain the contact loads (force and moments) at the interface corresponding to the unworn profile. The sum of contact loads at resonance, including the normal force N, the two tangential forces T_x and T_y, the two bending moments M_x and M_y and the torsional moment M_z, are then computed for each harmonic coefficient at the centre of the contact area. These loads are converted from the frequency domain into the time domain using an inverse discrete Fourier transform, so that the contact loads over one vibration cycle are obtained. Subsequently, the forces and moments are used as input for the contact solver to obtain the pressure, shear and slip fields at each time step of the fretting cycle. By enforcing the residuals of the conjugate gradient to be minimum within a given tolerance, the convergence of the solution is ensured for each time step. Once the

shear and slip fields are available at the contact interface, the wear depths are calculated at the contact interface using the energy wear approach. The wear which results from a single vibration cycle is too small to appreciate any noticeable change of the contact conditions, and consequently it would not impact the nonlinear dynamic response in any significant way. For that reason, a new contact analysis is performed again only after a certain number of cycles N_{cycles} are accumulated (wear iteration). This number of cycles, which represents a factor that makes the analysis faster, is defined as follows:

$$N_{\text{cycles}} = \text{floor}\left(\frac{\Delta h_{\max}}{\max \Delta h_{ij}}\right), \tag{2.7}$$

where $\Delta h_{\max}$ is the maximum allowed wear depth during one wear iteration and $\max \Delta h_{ij}$ is the maximum computed wear depth across the contact interface after one fretting cycle. It is worth noting that, based on this formula, each wear iteration can correspond to a different number of cycles. This factor is a very critical parameter of the analysis since it will determine the computational cost of the contact analysis, as well as the stability of the explicit scheme used to update the contacting surface profile with wear:

$$h_{ij} = h_{ij} + N_{\text{cycles}} \Delta h_{ij}. \tag{2.8}$$

A criterion based on the number of wear iterations or total wear volume is used to update the nonlinear dynamic model. Once an appropriate number of wear iterations has been performed, the 3D nonlinear contact elements are updated using the static pressure, gaps and stiffnesses obtained from the contact analysis of the worn profile. Subsequently, a new nonlinear dynamic response of the system is computed, which allows the extraction of contact forces for the contact analysis. The entire process is repeated until either the criterion of the maximum number of cycles or total wear volume is met.

Unlike the initial study performed in [25], the introduction of roughness at the contact interface in the present work allows the extraction of the contact stiffness values from the contact solver, which are then used to calibrate the penalty coefficients of the dynamic contact elements. Therefore, the stiffness distribution can be updated at each iteration as part of the multi-scale strategy, which is different compared to [25], where this distribution was assumed to be constant at the interface, and not evolving with the progression of wear.

3. Test case: resonator

The proposed multi-scale approach has been tested on resonator system with a single lap joint (figure 5) previously proposed and studied by Süß and Willner [34,35]. The set-up consists of two stainless steel masses which are connected with a bolted lap joint. The second mass is characterized by an 'o' shape, where one side is much thinner and therefore is acting as the elastic element in the system. The 3D FEM shown in figure 5 was run in Abaqus using a mesh of linear hex elements for the masses (19 504 elements) and the bolt (7830 elements). A tie constraint was applied in Abaqus to prevent any motion between the bolt heads and each mass and therefore the only frictional interface is the lap joint interface. The mode studied in this analysis is the first 'breathing' mode of the leaf spring shown in figure 5 as significant contact shear stresses are expected at the frictional interface. To allow a more physical interface for the wear analysis, a rough contact was generated at the lap joint interface. For this test case, a random surface with a Gaussian distribution was generated using an open source code provided by David Bergstrom [36]. Figure 6*a* shows an example of the Gaussian rough surface generated on a grid of 256 × 256 points for the lap joint interface.

Although other statistical distribution could be used, the choice of a Gaussian one seems reasonable as many freshly machined real surfaces exhibit it. Finally, the dynamic model was built, starting from the reduced linear models of the two halves of the resonator, and introducing a regular grid of nonlinear 3D contact elements at the interface (figure 6*b*). A total of 340 contact elements was used as a result of a compromise between the computational time and contact

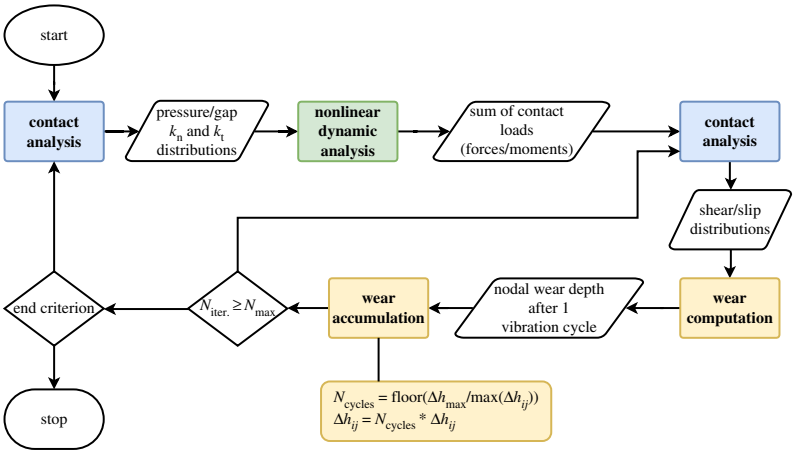

Figure 4. Detailed flow chart of the multi-scale modelling approach. (Online version in colour.)

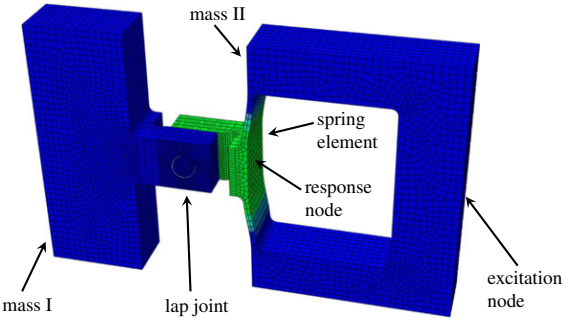

Figure 5. Visualization of the first breathing mode of the resonator. (Online version in colour.)

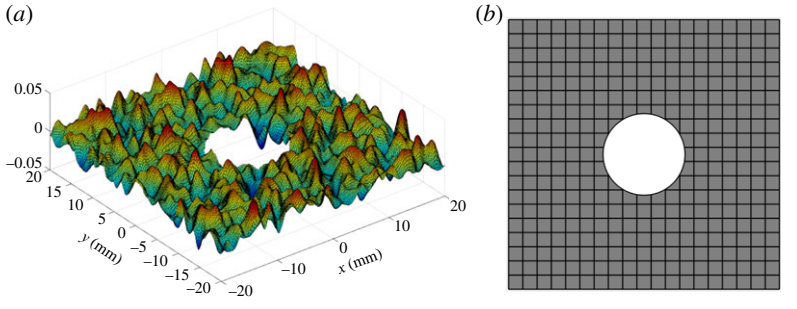

Figure 6. (*a*) Simulated rough surface for the joint interface (magnified roughness for visualization), (*b*) contact mesh used for the nonlinear dynamic analysis. (Online version in colour.)

refinement needed for the nonlinear dynamic analysis. Three harmonics plus the static term (harmonic 'zero') were used for the nonlinear dynamics analysis, as they were shown to be enough for capturing the contact nonlinearity. The main input parameters used for the subsequent simulations are reported in table 1. It is worth noting that the same linear elastic material is used for the entire structure. Therefore, the normal and tangential contact problems at the interface of the joint are uncoupled [30].

Table 1. Summary of the main input parameters for the linear dynamic model, contact model and nonlinear dynamic model.

linear dynamic model	
Young's modulus [GPa]	198.4
Poisson ratio	0.3
density [kg m^{-3}]	7949
contact analysis model	
nr. ele contact mesh	256 × 256
R_q roughness [μm]	0.5, 1, 5, 10
correlation length x, y [mm]	0.5
friction coefficient	0.6
nonlinear dynamic model	
nr. 3D contact element	340
nr. of harmonics	0, 1, 2, 3
nr. of modes in the reduced model	30

4. Results

In this section, the multi-scale modelling approach presented in §2, is applied to the test case of the single bolted joint resonator described in §3. Four different surfaces having an initial RMS roughness of 0.5, 1.0, 5.0 and 10 μm are analysed. Fretting wear simulations were run for each surface profile, up to 10 million vibration cycles, which was shown to be enough to reach a steady state. Fretting wear is having cascading effects on (a) the contact surface geometry (§2b), (b) the contact conditions (§2c) and (c) the nonlinear dynamic response (§2d). Owing to the fact that a similar behaviour was observed for all profiles, and to improve clarity, most of the results presented here are the ones associated with the profile having an initial RMS roughness of 5 μm.

(a) Input parameters

As described in §2, the wear simulations are controlled by two key parameters. The first one is the wear coefficient α that links the volume of wear to the frictional dissipated energy (see equation (2.5)). Owing to the lack of relevant experimental data, the wear coefficient used here is based on the previous work of Leonard [37], and is equal to 2×10^3 μm^3 J^{-1} for a steel-steel fretting contact. The second key parameter is the maximum allowed local wear depth per iteration. Its value must be small enough to ensure the stability of the wear scheme and at the same time as large as possible to speed up the computations. A value of 0.01 μm was found to be optimal for the profiles with an initial RMS roughness of 0.5 and 1 μm. A value of 0.1 μm has been used for the two other profiles. This second parameter leads to the use of an acceleration factor, which is the number of fretting cycles that can be accumulated before the maximum allowed local wear depth is attained, at which point the surface profile is updated and the refined contact analysis is performed again.

The other input data are the normal and tangential loads applied to the contact interface. Following the procedure described in §2e, an initial static contact analysis is performed by imposing a 30 kN load which simulates the axial force of the bolt. Subsequently, the dynamic analysis is run to extract the dynamic contact loads from the frequency response functions (FRFs) at resonance. The initial FRFs corresponding to each unworn rough surface under a 1000 N excitation are shown in figure 7. The necessary inputs for the contact analysis are the contact loads and displacements at resonance. More precisely, the input of the normal contact problem is the summation of the normal forces at each nonlinear friction element. For this particular test

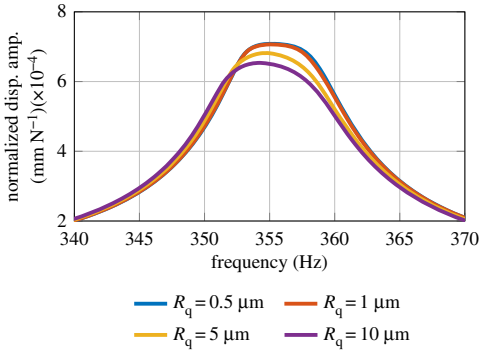

Figure 7. Initial FRFs for different initial RMS roughness. (Online version in colour.)

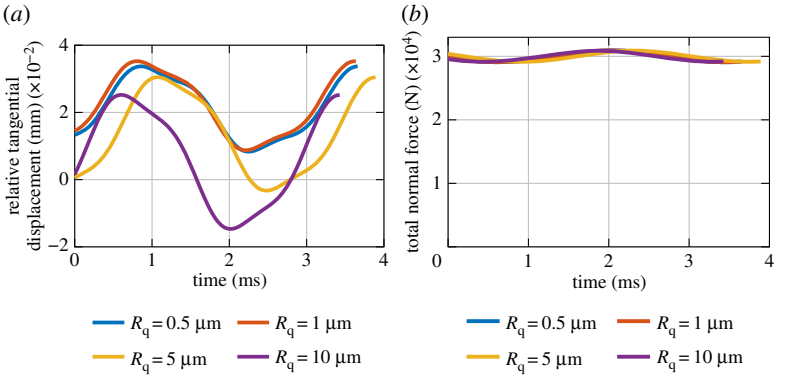

Figure 8. (*a*) Average tangential relative displacement at the joint interface, (*b*) total dynamic normal force at the joint interface. (Online version in colour.)

case, the bending moments were found to be negligible, as the mode excited is mainly causing shear stresses at the interface. The simulations of the tangential contact problem are displacement-controlled to allow macro-slip. The necessary input is therefore the average of the tangential relative motions over the contact interface. Before proceeding to the required summation and averaging, the data are converted from the frequency domain into the time domain using an inverse discrete Fourier transform. The resulting tangential and normal loadings, corresponding to each surface profile, are given in figure 8*a*,*b*.

As discussed in the authors' previous work [11], higher values of roughness lead to a more localized contact, which overall tends to lower the global stiffness of the interface. This generally was found to lead to larger relative tangential displacement, and in turn to higher energy dissipation. As for the normal contact, some significant changes could be observed in the local distribution across the interface depending on the initial value of roughness. Despite the local different distribution, the total normal load transmitted is equal to the bolt load (30 kN) plus a small harmonic oscillation due to the dynamic load, as shown in figure 8*b*. Using the input parameters described in this section, fretting wear simulations were run on each surface up to 10 million cycles at resonance frequency, without any update of the nonlinear dynamic model along the way. The effects of wear on the contact surface geometry and on the contact conditions are discussed in the next two sections.

(b) Effects of wear on the contact surface geometry

The first effect of wear is the change of the contacting surface geometry. Figure 9 shows the total wear depth obtained after 10 041 928 cycles for the profile having an initial RMS roughness

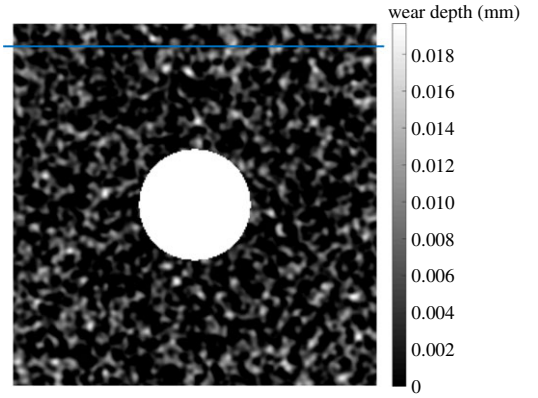

Figure 9. Cumulated wear depth in (millimetre) after 10 041 928 cycles, blue line: section of the profile. (Online version in colour.)

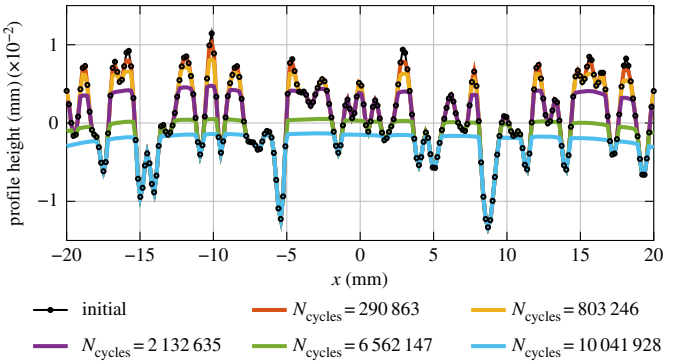

Figure 10. The evolution of surface profile with wear. Blue line section of figure 9. (Online version in colour.)

of 5 µm. The wear simulations were run using one CPU of an Intel Core i7-4700HQ 2.40 GHz. Each fretting cycle took approximately 70 s to run, but thanks to the acceleration factor, only 231 iterations were needed to reach 10 million cycles, which took approximately 4 h 29 min. Figure 10 shows the evolution of the surface profile with wear along the blue line drawn in figure 9.

It can be observed that due to the process of material removal caused by fretting wear, the higher peaks of the rough profile are progressively being flattened. Owing to this change of geometry, the roughness parameters of the surface are also affected, so that after only a few wear cycles, the four Gaussian rough surfaces used here are no longer Gaussian. In order to better describe the evolution of each surface, two additional roughness parameters, which are the skewness and kurtosis, will be used here as well. Skewness tells whether the shape of the surface height distribution is symmetric or skewed to one side. Its value can be computed using the following formula:

$$Sk = \frac{m_3}{m_2^{3/2}}, \tag{4.1}$$

where $m_3 = (1/n)\sum(h - \bar{h})^3$ and $m_2 = (1/n)\sum(h - \bar{h})^2$. $\bar{h}$ is the mean of the heights and n is the number of points. m_3 is called the third moment of the data and m_2 is the variance, i.e. the square of the standard deviation.

A Gaussian profile, being perfectly symmetric, is characterized by a skewness equal to 0. For non-Gaussian profiles, the skewness typically ranges from −2 to +2. The second parameter used to describe a non-Gaussian surface is the kurtosis which characterizes the sharpness of the central peak of the height distribution. High values of kurtosis are an indication of a higher and sharper

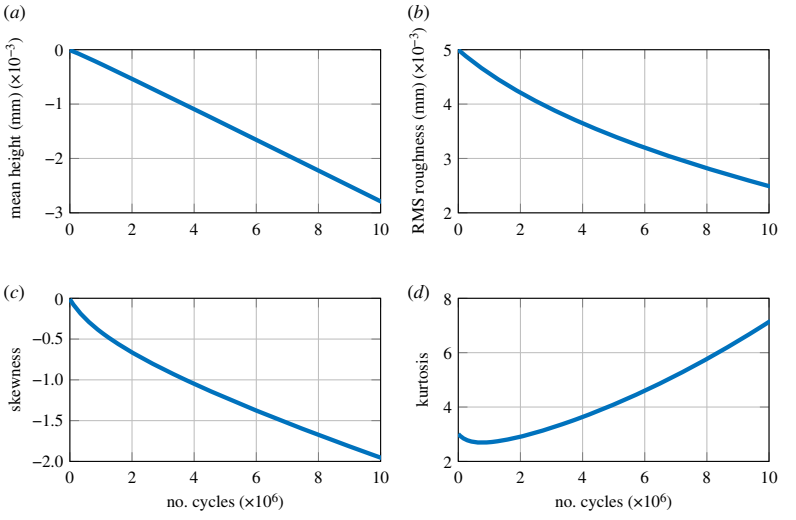

Figure 11. Evolution of (*a*) mean height, (*b*) RMS roughness, (*c*) skewness and (*d*) kurtosis with wear. (Online version in colour.)

central peak, whereas low values are an indication of a lower, less distinct peak. Kurtosis is linked to the fourth moment of the data m_4 via the following expression:

$$Ku = \frac{m_4}{m_2^2}, \tag{4.2}$$

where $m_4 = (1/n)\sum(h - \bar{h})^4$.

A Gaussian rough surface has a kurtosis equal to 3. A statistical analysis was carried out in order to show the evolution of the mean height, the RMS roughness, the skewness and the kurtosis of the lap joint surface with wear.

It can be seen that all roughness parameters of the surface are strongly affected by wear, as shown in figure 11. As the surface wears out, its RMS roughness tends to decrease. The couple skewness-kurtosis starts from (0,3), which is characteristic of a Gaussian rough surface, to different values, which confirms that the surface is no longer Gaussian. The evolution of the skewness indicates that the distribution of heights becomes negatively skewed as the surface wears out. This negative skewness is caused by the asymmetric effect of wear, which only affects the peaks of the profile (in contact), while the valleys (not in contact) maintain their shape. At the same time, due to the material removal, the profile distribution is closer to its mean value and therefore the kurtosis is increasing with wear (figure 11).

(c) Effects of wear on the contact conditions

The changes of contact geometry described in §4b have an impact on the contact conditions. In particular, the contact pressure is significantly affected, as shown by its evolution with wear in figure 12. As the surface wears out, the asperities are progressively removed, the contact area increases and consequently, the peaks of pressure are decreasing until nearly flat patches of much lower pressure are obtained.

The real contact area evolution for different values of initial RMS roughness is shown in figure 13. It can be observed, that smoother profiles start with a much larger real contact area compared with rougher profiles. In the range studied (up to 10 millions cycles), the smoother profiles are characterized by a more rapid initial increase followed by an asymptotic behaviour, compared to the rougher ones which exhibit a quasi-linear increase. Wear is also affecting another key parameter for the nonlinear dynamic analysis which is the contact stiffness. Figure 14*a* shows the evolution of the global normal contact stiffness for each rough profile. Two distinct phases can be observed: a running-in phase during which the contact stiffness rapidly increases and a

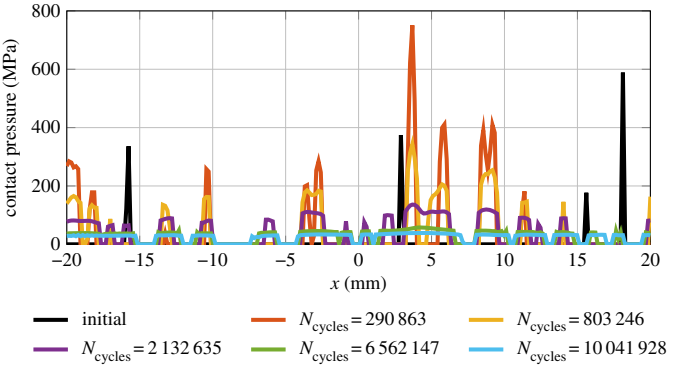

Figure 12. Evolution of contact pressure with wear. Blue line section of figure 9. (Online version in colour.)

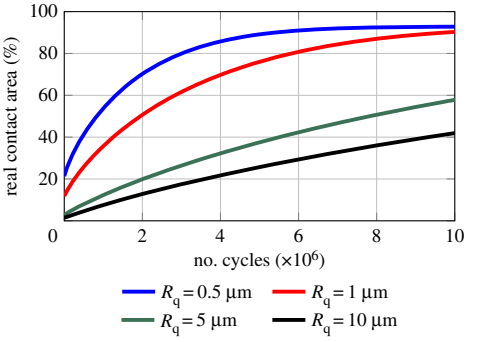

Figure 13. Evolution of contact area with wear. (Online version in colour.)

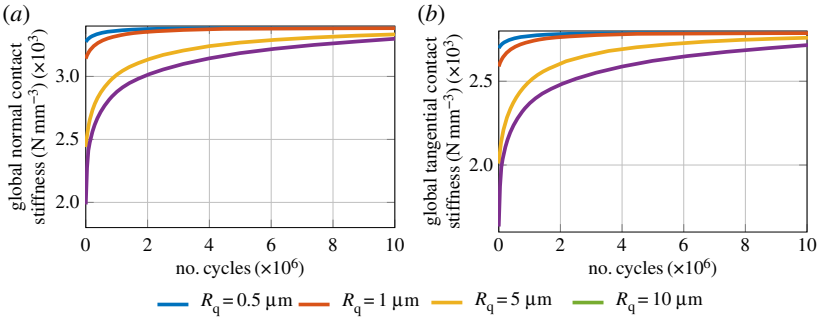

Figure 14. (*a*) Evolution of global normal contact stiffness with wear, (*b*) evolution of global tangential contact stiffness with wear. (Online version in colour.)

steady phase during which it keeps increasing, but at a much lower rate. During the running-in phase, there is an increasing number of asperities that come into contact which leads to more and more peaks of pressure which are associated with high values of contact stiffness. Then, as the peaks are progressively turning into larger patches of much lower pressure, the local values of contact stiffness are decreasing, but the overall contact stiffness keeps increasing because the global contact area does so. The results also seem to indicate that the global contact stiffness tends to the same value no matter what the initial RMS roughness is. The same observations can be made on the global tangential contact stiffness, which is plotted in figure 14*b*.

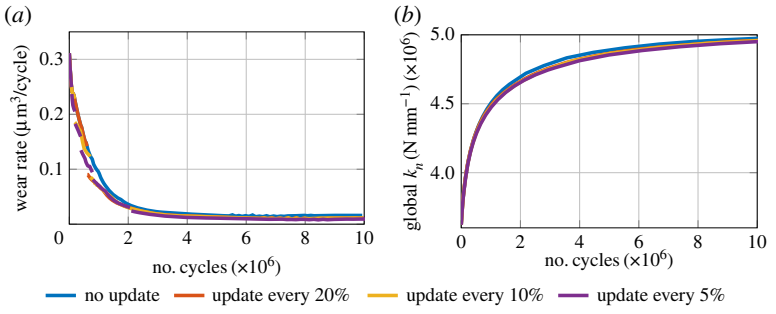

Figure 15. (*a*) Evolution of the wear rate for different update criteria, (*b*) evolution of global normal contact stiffness with wear for different update criteria. (Online version in colour.)

(d) Effects of wear on the nonlinear dynamics

(i) Criterion for the update of the nonlinear dynamic model

Up to this point, the coupling between fretting wear and nonlinear dynamics has been neglected. The nonlinear dynamic response depends on the local values of normal load, normal and tangential contact stiffness which drive the stick-slip phenomena taking place at the contact interface. However, in order to have one parameter usable as a criterion for the update of the nonlinear dynamic model, the global contact stiffness was chosen, leading to the following criterion: the nonlinear dynamic model, and more precisely the parameters of the friction elements which are the normal load, the gap and contact stiffness, are updated after a certain variation of the global contact stiffness is obtained in the wear simulations. The value of that variation depends on the system and the sensitivity of its dynamic behaviour to changes of contact conditions. For the present system, three values of 5, 10 and 20%, chosen arbitrarily, have been tested. Figure 15*a* shows the evolution of the wear rate for different update criteria of the nonlinear dynamic model. First of all, similar to the observations made on the contact stiffness, a running-in phase and a steady phase can be observed. Secondly, a jump in the wear rate is obtained after each update of the nonlinear dynamic model. This can be explained by the fact that the increase of contact stiffness with wear leads to smaller tangential relative displacements at the contact interface, and therefore to a lower energy dissipation, and a lower wear rate. The influence of the update is noticeable in the running-in phase, during which the largest differences can be observed between the blue curve and the others. But these differences nearly vanish during the steady-state wear: after only one million cycles, the three update criteria are yielding to nearly the same wear rate. Figure 15*b* depicts the evolution of the contact stiffness for the different update criteria. As can be seen, the global contact stiffness is barely affected by the updates, and all of them are yielding to nearly the same stiffness during all simulated cycles. Based on these observations, the nonlinear dynamic response after these 10 million cycles is expected to be the same for all update criteria, which is confirmed by the FRFs shown in figure 16.

As a result, for this particular test case, no update of the nonlinear dynamic model is needed to discuss the effects of roughness and wear on the dynamic response up to 10 million cycles. This indicates that the coupling between the contact evolution and dynamics is minimal. For that reason, all subsequent presented results have been obtained without updating the nonlinear dynamic model.

(ii) Effects of wear on the nonlinear dynamics

Finally, the impact of fretting wear on the dynamic response of the system was analysed, and the FRFs at different number of cycles are shown in figure 17*a*. The results discussed in §2c, where surface roughness was seen to decrease due to the fretting process, can help to explain the behaviour observed here. In fact, this loss of roughness results in a global stiffening of the contact

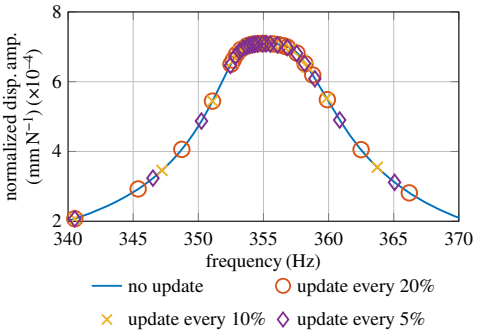

Figure 16. FRFs after 10 million cycles for different update criteria. (Online version in colour.)

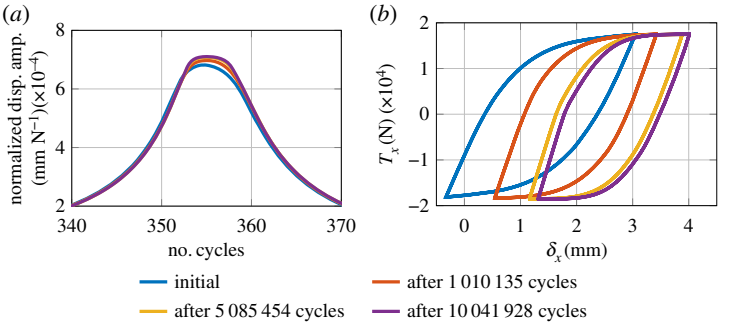

Figure 17. (*a*) Evolution of FRFs with wear for $R_q = 5$ µm, (*b*) evolution of dissipated energy per cycle with wear for $R_q = 5$ µm. (Online version in colour.)

interface, which drives the slight tendency towards higher resonance frequencies observed in figure 17*a*. At the same time, a higher amplitude of the FRFs can be observed with the wear progressing, which indicates a lower energy dissipation due to friction at the contact interface. To better understand this energy dissipation mechanism, the contact hysteresis loops due to the oscillatory loading were extracted for the whole contact interface, as shown in figure 17*b*. As the number of fretting cycle increases, the stick part of the loop increases its slope (stiffness), and the micro-slip transition to sliding becomes sharper, leading to a lower enclosed area of the cycle (energy dissipated). A clear shift of the loops due to the static component of the dynamic response can be observed as well. Figure 18*a* shows the FRFs of the worn surfaces obtained after 10 million cycles. By comparing it with figure 7, it can be observed that due to wear, the responses are getting closer to each other and are nearly identical after 10 million cycles. This result is supported by figure 14*a* and figure 18*b* which show that after 10 million cycles, all initial rough surfaces tend to have similar global contact stiffness and wear rate. It can also be observed from figure 18*b*, that the higher the initial RMS roughness, the higher the wear rates, and that the wear rate decreases to a steady-state value, which has been previously observed by Ghosh & Sadeghi [38]. These findings have also been observed experimentally by Kubiak *et al.* [39].

(iii) Effects of plasticity

Surface roughness reduces significantly the real area of contact and therefore leads to localized peaks of pressure. These local pressures can exceed the yield strength of the material and thus plasticity may occur on the contacting surfaces and inside the bulk materials. In order to take into account plasticity in the contact analysis, a very simple elastic-perfectly-plastic model, previously used by Spinu [40], has been implemented here. It consists in preventing the contact pressure from exceeding the yield strength of the material. As a result, the constraint that must be enforced

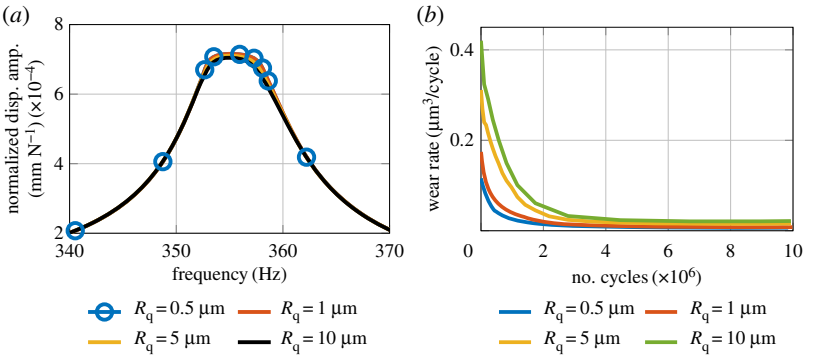

Figure 18. (*a*) Final FRFs for different initial RMS roughness, (*b*) wear rates for different initial RMS roughness. (Online version in colour.)

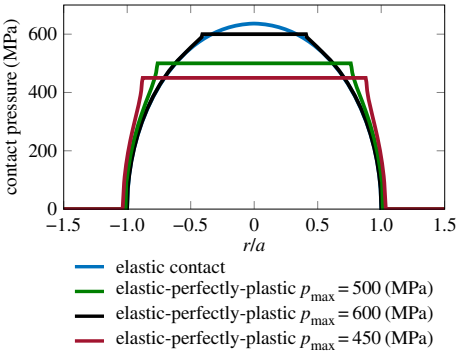

Figure 19. Computed pressure for elastic and elastic-perfectly-plastic contact. (Online version in colour.)

on the contact pressure in the algorithm is now:

$$\left.\begin{aligned} &p_{\max} \geq p_{ij} \geq 0,\ g_{ij} = 0,\ (i,j) \in A_C \\ \text{and} \quad &p_{ij} = 0,\ g_{ij} \geq 0,\ (i,j) \notin A_C, \end{aligned}\right\} \tag{4.3}$$

where $p_{\max}$ is the compressive yield strength of the material. In order to illustrate the effects of this modification to the contact algorithm, a Hertzian contact is studied here by adding a maximum pressure value. Figure 19 shows the contact pressure obtained for the elastic contact, and for the elastic-perfectly-plastic contact for three different values of limiting pressure (600 [MPa], 500 [MPa] and 450 [MPa]). A circular region of plasticity, in which the pressure is equal to the imposed limited value, is observed and leads to a redistribution of contact pressure in the elastic region surrounding it. A small extension of the overall contact area can also be observed. These results are consistent with the ones obtained by Spinu [40]. The same approach has been used here to evaluate the potential influence of plasticity on the wear analysis of the lap joint rough interface with an initial RMS roughness of 5 μm. The hardness limit was set to 600 MPa, which is an average value of compressive yield strength for steel materials. Figure 20 shows the initial pressure distribution for the elastic, and the elastic-perfectly-plastic contacts. It can be seen that the pressure distribution is strongly affected by the hardness limit: the numerous peaks that were higher than 600 MPa in the elastic contact, are now all equal to 600 MPa. Similarly to the Hertzian contact case, a slight increase of contact area could be observed, as shown in figure 21*a*. Another parameter which is affected by plasticity is the normal contact stiffness, as shown in figure 21*b*. When the asperities reach the plastic limit, their stiffness tend to drop, but at the same time, more and more asperities come into contact due to the re-distribution of contact pressure. These new asperities in contact will partially contrast this tendency of decrease in stiffness due to plasticity.

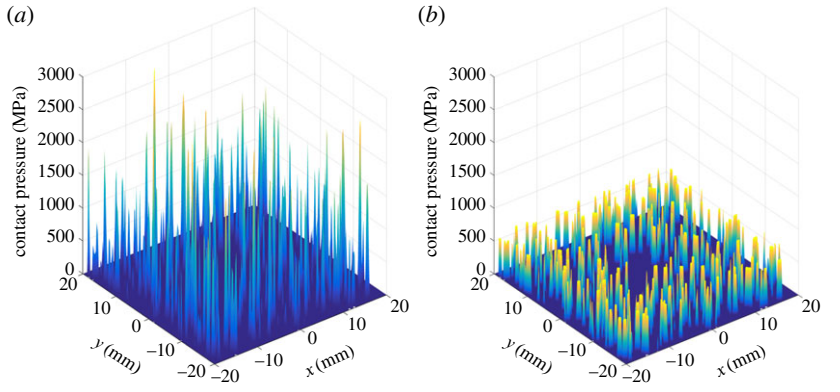

Figure 20. Initial contact pressure [MPa] for the elastic (*a*) and elastic-perfectly-plastic with $p_{max} = 600$ MPa (*b*) contact. (Online version in colour.)

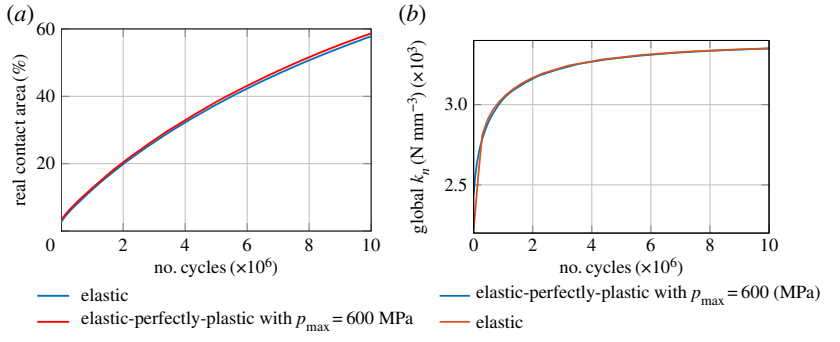

Figure 21. (*a*) Evolution of real contact area with wear for elastic and elastic-perfectly-plastic behaviour, (*b*) evolution of global normal contact stiffness with wear for elastic and elastic-perfectly-plastic behaviour. (Online version in colour.)

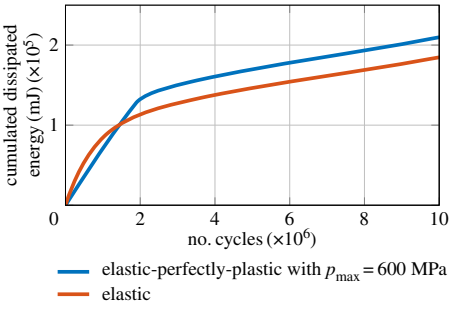

Figure 22. Cumulated dissipated energy for elastic and elastic-perfectly-plastic behaviour. (Online version in colour.)

Looking at the stiffness evolution with wear shown in figure 21*b*, it is clear that in the initial phase, when the surface roughness is still high, the contact with plasticity exhibits lower stiffness. As the fretting cycles increase, and some roughness is lost due to wear, the global stiffness tend to become nearly equal to the elastic case, since less and less asperities reach the plastic limit, as previously shown in figure 12 of §c. Similar observations can be made on the evolution of the cumulated dissipated energy, depicted in figure 22. In fact, the wear rates, which are equal to the slope of these curves multiplied by the wear coefficient, show a significantly different behaviour during the initial phase, until they reach a similar value after approximately 2 million cycles.

Therefore, these results suggest that a more realistic contact analysis which includes plasticity should be performed in case the initial running-in phase is of particular interest for the study.

5. Conclusion

In this paper, a novel multi-scale method is presented to model the effect of fretting wear on the nonlinear dynamics of assembled structures. The proposed approach uses a multi-harmonic balance solver for the dynamics of the system, and a BEM-based contact solver in conjunction with an energy wear approach for the fretting wear analysis. Two different time scales are used, a fast one for dynamics and a slow one for contact. Similarly, two space scales are introduced to allow a refined mesh for the contact analysis, while keeping a coarser mesh for the dynamics. As a result of this, surface roughness can be directly included in the contact analysis, allowing a more physical description of the wear evolution.

The modelling approach is then evaluated on a single bolted joint resonator with a rough contact interface. Fretting wear is first shown to have a strong impact on the contacting surface geometry, and in turn, affecting the contact conditions. In fact, an increase of contact area, and a re-distribution of contact pressure is observed, which leads to an overall increase of the contact stiffness of the interface. In order to evaluate the coupling between the contact and dynamic analyses, a criterion which allows to update the dynamic model after a certain variation of the global contact stiffness is proposed as well. For the present application, it is found that the coupling is very low, as the different update values tested do not result in any noticeable change of the nonlinear dynamic response of the system. From a wear perspective, higher wear rates are observed for higher values of initial roughness, which result in initial significant differences between the various surfaces tested. However, after the loss of the initial roughness due to wear, a steady-state phase can be observed during which the wear rates reach nearly the same value for all surfaces.

Finally, the evolution of the nonlinear dynamics of the system with wear is evaluated. A slight increase of the resonance frequency can be observed, which is driven by the stiffening of the contact interface. This frequency shift is also accompanied by a slightly higher amplitude of response due to a lower energy dissipation at the frictional interface. The effect of plasticity is also briefly analysed using a simplified approach based on the introduction of a hardness limit in the contact solver. As a result of the plastic limit, a difference in terms of pressure distribution and stiffness is observed in the initial phase, which then vanishes at a higher number of fretting cycles.

Data accessibility. This article has no additional data.

Authors' contributions. J.A. implemented the numerical tools and performed the simulations. L.P. and J.A. wrote the paper. L.S. and C.W.S. defined the research project. All authors contributed to various aspect of the research discussing directions to take and suggesting ideas.

Competing interests. We declare we have no competing interests.

Funding. This work is part of a collaborative R & T project SILOET II P19.6 which is co-funded by Innovate UK and Rolls-Royce plc and carried out by Rolls-Royce plc and the Vibration UTC at Imperial College London.

References

1. Petrov EP, Ewins DJ. 2004 State-of-the-art dynamic analysis for non-linear gas turbine structures. *Proc. Inst. Mech. Eng. G: J. Aerosp. Eng.* **218**, 199–211. (doi:10.1243/0954410041872906)
2. Gaul L, Nitsche R. 2001 The role of friction in mechanical joints. *Appl. Mech. Rev.* **54**, 93–106. (doi:10.1115/1.3097294)
3. Krack M, Salles L, Thouverez F. 2016 Vibration prediction of bladed disks coupled by friction joints. *Arch. Comput. Methods Eng.* **24**, 589–636. (doi:10.1007/s11831-016-9183-2)
4. Griffin JH. 1980 Friction damping of resonant stresses in gas turbine engine airfoils. *J. Eng. Power* **102**, 329–333. (doi:10.1115/1.3230256)

5. Mea B. 2018 Reduced order modeling of nonlinear structures with frictional interfaces. In *The mechanics of jointed structures*. Berlin, Germany: Springer.
6. Panning L, Sextro W, Popp K. 2003 Spatial dynamics of tuned and mistuned bladed disks with cylindrical and wedge-shaped friction dampers. *Int. J. Rotating Mach.* **9**, 219–228. (doi:10.1155/S1023621X03000198)
7. Fantetti A, Gastaldi C, Berruti T. 2018 Modeling and testing friction flexible dampers: challenges and peculiarities. *Exp. Tech.* **42**, 407–419. (doi:10.1007/s40799-018-0248-z)
8. Csaba G. 1999 Modelling of a microslip friction damper subjected to translation and rotation. In *Proc. of ASME Gas Turbine and Aeroengine Congress and Exhibition*, vol. 4, p. V004T03A012.
9. Gastaldi C, Gola MM. 2016 On the relevance of a microslip contact model for under-platform dampers. *Int. J. Mech. Sci.* **115–116**, 145–156. (doi:10.1016/j.ijmecsci.2016.06.015)
10. Pesaresi L, Armand J, Schwingshackl C, Salles L, Wong C. 2018 An advanced underplatform damper modelling approach based on a microslip contact model. *J. Sound Vib.* **436**, 327–340. (doi:10.1016/j.jsv.2018.08.014)
11. Armand J, Salles L, Schwingshackl C, Süß D, Willner K. 2018 On the effects of roughness on the nonlinear dynamics of a bolted joint: a multiscale analysis. *Eur. J. Mech. A Solids* **70**, 44–57. (doi:10.1016/j.euromechsol.2018.01.005)
12. Archard JF. 1953 Contact and rubbing of flat surfaces. *J. Appl. Phys.* **24**, 981. (doi:10.1063/1.1721448)
13. Fouvry S, Liskiewicz T, Kapsa P, Hannel S, Sauger E. 2003 An energy description of wear mechanisms and its applications to oscillating sliding contacts. *Wear* **255**, 287–298. (doi:10.1016/S0043-1648(03)00117-0)
14. Zmitrowicz A. 2006 Wear patterns and laws of wear—a review. *J. Theor. Appl. Mech.* **44**, 219–253.
15. Bryant MD, Khonsari MM, Ling FF. 2008 On the thermodynamics of degradation. *Proc. R. Soc. A* **464**, 2001–2014. (doi:10.1098/rspa.2007.0371)
16. McColl IR, Ding J, Leen SB. 2004 Finite element simulation and experimental validation of fretting wear. *Wear* **256**, 1114–1127. (doi:10.1016/j.wear.2003.07.001)
17. Rodríguez-Tembleque L, Abascal R, Aliabadi M. 2012 Anisotropic fretting wear simulation using the boundary element method. *Comput. Model. Eng. Sci.* **87**, 127–156. (doi:10.3970/cmes.2012.087.127)
18. Leonard BD, Ghosh A, Sadeghi F, Shinde S, Mittelbach M. 2014 Third body modeling in fretting using the combined finite-discrete element method. *Int. J. Solids Struct.* **51**, 1375–1389. (doi:10.1016/j.ijsolstr.2013.12.036)
19. Aghababaei R, Warner DH, Molinari JF. 2016 Critical length scale controls adhesive wear mechanisms. *Nat. Commun.* **7**, 11816. (doi:10.1038/ncomms11816)
20. Sextro W. 2007 *Dynamical contact problems with friction*. Berlin/Heidelberg/New York: Springer Science + Business Media.
21. Pettigrew M, Taylor C. 2003 Vibration analysis of shell-and-tube heat exchangers: an overview—Part 2: vibration response, fretting-wear, guidelines. *J. Fluids Struct.* **18**, 485–500. (doi:10.1016/j.jfluidstructs.2003.08.008)
22. Jareland MH, Csaba G. 2000 Friction damper mistuning of a bladed disk and optimization with respect to wear. In *Manufacturing materials and metallurgy, ceramics, structures and dynamics, controls, diagnostics and instrumentation, education*, vol. 4. New York: ASME.
23. Petrov EP. 2013 Analysis of nonlinear vibrations upon wear-induced loss of friction dampers in tuned and mistuned bladed discs. In *Structures and dynamics*, vol. 7A. New York: ASME.
24. Salles L, Blanc L, Thouverez F, Gouskov A. 2011 Dynamic analysis of fretting-wear in friction contact interfaces. *Int. J. Solids Struct.* **48**, 1513–1524. (doi:10.1016/j.ijsolstr.2011.01.035)
25. Armand J, Pesaresi L, Salles L, Schwingshackl C. 2016 A multiscale approach for nonlinear dynamic response predictions with fretting wear. *J. Eng. Gas Turbines Power* **139**, 022505-1–022505-7. (doi:10.1115/1.4034344)
26. Petrov EP, Ewins DJ. 2003 Analytical formulation of friction interface elements for analysis of nonlinear multi-harmonic vibrations of bladed disks. *J. Turbomach.* **125**, 364–371. (doi:10.1115/1.1539868)
27. Petrov EP. 2011 A high-accuracy model reduction for analysis of nonlinear vibrations in structures with contact interfaces. *J. Eng. Gas Turbines Power* **133**, 102503. (doi:10.1115/1.4002810)

28. Salles L, Blanc L, Thouverez F, Gouskov A, Jean P. 2012 Dual time stepping algorithms with the high order harmonic balance method for contact interfaces with fretting-wear. *J. Eng. Gas Turbines Power* **134**, 032503 (1–7). (doi:10.1115/1.4004236)
29. Armand J, Salles L, Schwingshackl CW. 2015 Numerical simulation of partial slip contact using a semi-analytical method. In *ASME 2015 Int. Design Engineering Technical Conf. and Computers and Information in Engineering Conference*, pp. V008T13A022–V008T13A022.
30. Polonsky IA, Keer LM. 2000 Fast methods for solving rough contact problems: a comparative study. *J. Tribol.* **122**, 36–41. (doi:10.1115/1.555326)
31. Johnson KL. 1985 *Contact mechanics*. Cambridge, UK: Cambridge University Press. Cambridge Books Online.
32. Love AEH. 1906 *A treatise on the mathematical theory of elasticity*. A Treatise on the Mathematical Theory of Elasticity. Cambridge, UK: Cambridge University Press.
33. Ramalho A, Miranda J. 2006 The relationship between wear and dissipated energy in sliding systems. *Wear* **260**, 361–367. (doi:10.1016/j.wear.2005.02.121)
34. Süß D. 2016 *Multi-Harmonische-Balance-Methoden zur Untersuchung des Übertragungsverhaltens von Strukturen mit Fügestellen*. PhD thesis Dissertation, Erlangen, Friedrich-Alexander-Universität Erlangen-Nürnberg (FAU).
35. Süß D, Willner K. 2015 Investigation of a jointed friction oscillator using the Multiharmonic Balance Method. *Mech. Syst. Signal Process.* **52-53**, 73–87. (doi:10.1016/j.ymssp.2014.08.003)
36. Bergstrom D. 2010 Rough surface generation and analysis [online], Available from http://www.mysimlabs.com/surface_generation.html.
37. Leonard BD. 2008 An experimental and numerical investigation of the effect of coatings and third body on fretting wear. PhD thesis, Purdue University.
38. Ghosh A, Sadeghi F. 2015 A novel approach to model effects of surface roughness parameters on wear. *Wear* **338-339**, 73–94. (doi:10.1016/j.wear.2015.04.022)
39. Kubiak K, Liskiewicz T, Mathia T. 2011 Surface morphology in engineering applications: influence of roughness on sliding and wear in dry fretting. *Tribol. Int.* **44**, 1427–1432. (doi:10.1016/j.triboint.2011.04.020)
40. Ioan U, Sergiu S. 2010 A simplified model for pressure distribution in elastic-perfectly plastic contacts. *Ann. Oradea Univ.* **XIX**, 2010/2. (doi:10.15660/AUOFMTE.2010-2.1895)